Human Molecular Genetics, 2018, Vol. 27, No. 1 147–159

doi: 10.1093/hmg/ddx392
Advance Access Publication Date: 31 October 2017
Original Article

ORIGINAL ARTICLE

Changes in extracellular matrix cause RPE cells to make basal deposits and activate the alternative complement pathway

Rosario Fernandez-Godino[1,2], Kinga M. Bujakowska[1,2] and Eric A. Pierce[1,2,*]

[1]Department of Ophthalmology, Massachusetts Eye and Ear Infirmary, Ocular Genomics Institute, Boston, MA 02114, USA and [2]Harvard Medical School, Boston, MA 02114, USA

*To whom correspondence should be addressed at: Massachusetts Eye and Ear Infirmary, Ocular Genomics Institute, 243 Charles Street, Boston, MA 02114, USA. Tel: +1 6175736917; Fax: +1 6175736920; Email: eric_pierce@meei.harvard.edu

Abstract

The design of efficient therapies for age-related macular degeneration (AMD) is limited by our understanding of the pathogenesis of basal deposits, which form between retinal pigment epithelium (RPE) and Bruch's membrane (BrM) early in disease, and involve activation of the complement system. To investigate the roles of BrM, RPE and complement in an AMD, we generated abnormal extracellular matrix (ECM) using CRISPR-edited ARPE-19 cells. We introduced to these cells the p.R345W mutation in *EFEMP1*, which causes early-onset macular degeneration. The abnormal ECM binds active complement C3 and causes the formation of basal deposits by normal human fetal (hf)RPE cells. Human fetal RPE (hfRPE) cells grown on abnormal ECM or BrM explants from AMD donors show chronic activation of the alternative complement pathway by excessive deposition of C3b. This process is exacerbated by impaired ECM turnover via increased matrix metalloproteinase-2 activity. The local cleavage of C3 via convertase-independent mechanisms can be a new therapeutic target for early AMD.

Introduction

Age-related macular degeneration (AMD) is the most common cause of blindness among elderly people, but the design of effective therapies for AMD is limited by the lack of knowledge regarding the mechanisms associated with early steps in disease (1). Currently available treatments target intermediate/late stages of disease. For example, antioxidant supplementation can slow AMD progression in some patients with intermediate disease (2), and the development of anti-VEGF therapies has been a major advance in the treatment of choroidal neovascularization associated with late stage disease (1). However, there are no effective therapies available to prevent progression of early AMD, when basal deposits and drusen form between the basal lamina of the retinal pigment epithelium (RPE) and Bruch's membrane (BrM), to the later vision-threatening stages of disease.

Aging causes degeneration and thickening of BrM by accumulation of extracellular matrix (ECM) structural components and impaired matrix metalloproteinase (MMP) activity, which is thought to be exacerbated by both genetic and environmental factors in AMD (3–7). Importantly, RPE cells synthesize MMP-2, which is key for ECM remodeling in BrM (8,9), and dysregulation of which triggers inflammatory processes associated with the development of AMD, likely via cleavage and regulation of chemokines, ECM proteins and their regulators (4,6,10–12). But identification of the specific factors and mechanisms that lead from basal deposits to drusen formation and then to progression of AMD remain to be defined.

Experimental and clinical evidence strongly indicate a role for the complement system in AMD as early as drusen formation (13–19). Nonetheless, several anti-complement drugs that target specific complement pathways have been developed and tested in clinical trials without significant success to date

Received: August 1, 2017. **Revised:** October 4, 2017. **Accepted:** October 25, 2017

(20–22). For example, Compstatin, a peptide that inhibits activation of C3-convertase did not show efficacy in Phase II Clinical Trials (23,24) (Clin Trial NCT01603043). This is a noteworthy result because activation of C3 is a common endpoint of all three complement pathways (classical, lectin and alternative) (25).

The design of effective complement-modulating therapies for AMD requires a better understanding of direct functional connections between alterations in the complement system and the pathogenesis of macular degeneration. Also, there is controversy about which pathway triggers complement activation in AMD and if this process is local or systemic (14,26,27). We previously demonstrated that abnormalities in the ECM are associated with local activation of complement by the RPE in a mouse model of inherited macular degeneration (28–30). However, the specific complement pathway responsible for this process and the basis of the connection between altered ECM and complement activation remains to be defined.

Genetic association studies have identified risk alleles for AMD in genes that encode multiple complement system components (15,16). The majority of these risk alleles, and the majority of complement components found in the BrM and drusen of AMD patients belong to the alternative pathway (15,16,18,31). Under normal conditions, the complement system is constantly activated by the tick-over process at a low level. In this way, C3 is cleaved by physiological hydrolysis of its internal thioester, generating free hydrolyzed complement 3 [C3(H2O)] and C3a (32,33). C3(H2O) deposited on the ECM can form a stable properdin-independent C3(H2O)-convertase capable of activating the alternative pathway, generating more C3b, which in turn creates a positive feedback loop that will result in the increased release of the anaphylatoxin C3a (34–36). This process cannot be regulated by CFH (33,37,38) or inactivated by Compstatin, which may explain the inefficiency of this drug in AMD patients (23).

The *EFEMP1*-associated macular degeneration, caused by the dominant p.R345W mutation in the EGF-containing fibulin-like ECM protein 1 (EFEMP1) shares clinical features with AMD, such as the presence of basal deposits and drusen (39,40). Moreover, EFEMP1 protein has been demonstrated to accumulate beneath the RPE overlaying drusen and basal deposits in AMD patients (41–43). We previously demonstrated that primary RPE cells from *Efemp1*$^{R345W/R345W}$ mutant mice make basal deposits *in vitro* and activate complement locally (30). To further investigate how alterations in the ECM increase activation of the complement system in early macular degeneration, we generated human ARPE-19 cells with the pathogenic p.R345W mutation in the *EFEMP1* gene, and studied the response of normal human fetal (hf) RPE cells to the abnormal ECM made by the mutant ARPE-19 cells. We also investigated the response of normal hfRPE cells to BrM from eyes with AMD. The data obtained from these studies show that abnormalities in the structure and composition of the ECM, caused either by the p.R345W mutation in EFEMP1 or associated with AMD, are sufficient to produce increased complement activation and basal deposit formation by normal RPE cells. The data further suggest that C3 produced by RPE cells is likely activated via tick-over and deposited in excess on abnormal ECM, where it causes a local chronic activation of the alternative complement pathway. To our knowledge, this is the first demonstration that the alternative complement pathway is responsible for the local activation of complement in AMD. Moreover, the data reported show that the abnormal structure of ECM/BrM can initiate the local activation of the complement system as one of the early steps in the pathogenesis of AMD, and that this mechanism is shared between an inherited macular degeneration and AMD.

Results

Generation of ARPE-19 cells that harbor the mutation c.1033C>T (p.R345W) in the EFEMP1 gene via CRISPR–Cas9 editing

We have previously demonstrated that primary mouse RPE cells carrying the mutation p.R345W (c.1033C>T) in the *Efemp1* gene make basal deposits *in vitro* (30). Given that *EFEMP1*-associated macular degeneration is an ultra-rare disease, it is difficult to obtain samples from affected patients to use for studies of basal deposit formation *in vitro* by mutant human RPE cells. However, genome editing using the Clustered regularly interspaced short palindromic repeats (CRISPR)–Cas9 system allows the assessment of functional consequences of single risk alleles on the cellular phenotype in an isogenic background (44). Hence, we engineered ARPE-19 cells to be homozygous for c.1033C>T mutation in exon 9 of the *EFEMP1* gene (Fig. 1A).

Genome editing with wild-type CRISPR–Cas9 relies on a double strand break (DSB) introduced by the Cas9 nuclease. The ability to precisely target a specific site is critical, because point mutations are generated via homology directed repair (HDR) with a single stranded donor oligonucleotide (ssODN), which carries the desired change (44,45). We generated a DSB after the nucleotide base 1033, which coincides with the site of mutation. We co-transfected the cells with the pSpCas9(BB)-2A-GFP (PX458) plasmid carrying the Cas9 nuclease and guide RNA (gRNA) with the ssODN harboring the desired mutation c.1033C>T. A silent mutation was introduced to change the PAM sequence of the ssODN, so the targeted allele cannot be recognized by the nuclease after HDR (Fig. 1A and B).

A total of 2208 transfected cells were plated into 96-well plates, and 937 clones derived from single cells were expanded for further analyses. In general, the efficiency of HDR using CRISPR/Cas9 is quite low owing to the preferential non-homologous end joining (NHEJ) of DNA ends. However, treatment with the ligase IV inhibitor SCR7 increased the efficiency of the HDR over the NHEJ resulting in more than 25% of the total clones screened carrying the c.1033C>T mutation in one or two alleles (Fig. 1C). More than 11% of clones had at least one copy of the mutation with no evidence off-target variation, and 4.4% of them had two copies of the mutation after a single round of transfection (Fig. 1C and D). In some cases, HDR was successful but either one or both alleles also included a small indel (usually one to eight bases) that generated hemizygous *EFEMP1*$^{WT/-}$ (WT/–), *EFEMP1*$^{R345W/-}$ (KI/–) or knock-out *EFEMP1*$^{-/-}$ (–/–) cells. Hemizygous KI/– that harbor the mutation in one or both alleles plus indels in one allele were only found in the samples treated with SCR7 (Fig. 1D). Moreover, the treatment with SCR7 appeared to favor the formation of out-of-frame indels at the expense of in-frame indels (Fig. 1E).

The presence of predicted potential off-target alterations was ruled out by Sanger sequencing (see Methods section). Only one clone presented an intronic point mutation A>G (chr13: +71022300) that did not affect the cDNA sequence. This clone was not used for further experiments.

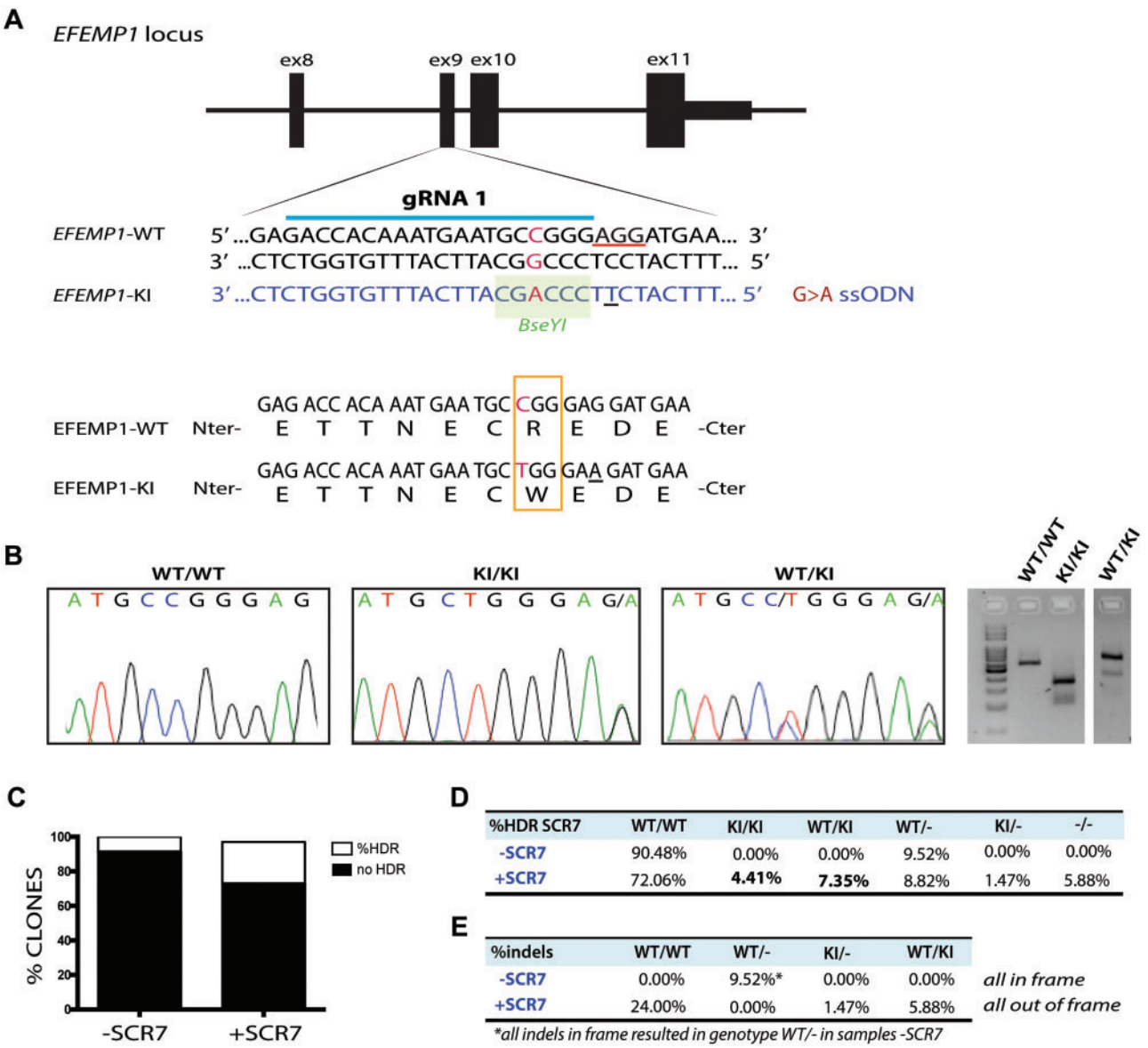

%HDR SCR7	WT/WT	KI/KI	WT/KI	WT/-	KI/-	-/-
-SCR7	90.48%	0.00%	0.00%	9.52%	0.00%	0.00%
+SCR7	72.06%	**4.41%**	**7.35%**	8.82%	1.47%	5.88%

%indels	WT/WT	WT/-	KI/-	WT/KI	
-SCR7	0.00%	9.52%*	0.00%	0.00%	*all in frame*
+SCR7	24.00%	0.00%	1.47%	5.88%	*all out of frame*

**all indels in frame resulted in genotype WT/- in samples -SCR7*

Figure 1. Knock-in the mutation p.R345W in the EFEMP1 gene via CRISPR–Cas9. (**A**) Design of guide RNA (gRNA) and single strand oligonucleotide donor (ssODN) to knock-in the mutation c.1033C>T in the exon 9 of the *EFEMP1* gene in ARPE-19 cells via CRISPR–Cas9. PAM sequence underlined in red. Change G>A in the ssODN creates a new restriction site for the *BseYI* enzyme (highlighted in green). (**B**) Sanger sequence and agarose gel of successfully edited and isolated clones with genotype WT/WT (wild-type), KI/KI (two copies of the mutation, one per allele) and WT/KI (only one allele has the mutation). (**C**) Percentage of clones that had the mutation, comparing untreated (−SCR7) and treated (+SCR7) with the DNA ligase IV inhibitor SCR7. (**D**) Quantification of edited clones according to their genotype: WT/WT: both alleles wild-type; KI/KI: both alleles mutant; WT/KI: one allele mutant and one WT; WT/−: one allele wild-type and one allele with indels that result in null allele; KI/−: one allele with the mutation and one allele with indels that result in null allele; −/−: both alleles have indels that result in null alleles. (**E**) Percentage of clones treated with or without SCR7 which alleles had indels in frame or out of frame.

CRISPR–Cas9 edited ARPE-19-EFEMP1$^{R345W/R345W}$ cells make abnormal ECM in vitro

Our previous experiments using primary RPE cells from *Efemp1*$^{R345W/R345W}$ mice demonstrated that the p.R345W mutation in EFEMP1 causes abnormalities in the structure and turnover of the ECM as well as to the activation of complement *in vitro* (30). We hypothesized that edited ARPE-19-*EFEMP1*$^{R345W/R345W}$ cells can make abnormal ECM that is similar to the altered BrM found in AMD patients and that precede basal deposits and drusen. We cultured ARPE-19 wild-type and ARPE-19-*EFEMP1*$^{R345W/R345W}$ mutant cells on transwells in RPE media in the absence of serum (30,46) (Supplementary Material, Fig. S1). After 4 weeks, decellularization of the transwells was performed and the exposed ECM was fixed and imaged by scanning electron microscopy (SEM). SEM images showed that the structure of the ECM generated by the mutant cells was abnormal, with elongated fibers that covered most of the transwell, while the ECM generated by the wild-type cells was organized in a distinct pattern (Fig. 2A–D).

Immunostaining for the main components of basal laminar deposits in AMD patients, such as EFEMP1, laminin, fibronectin, collagen IV and VI (5,41,47), confirmed that the abnormal ECM was comprised of these proteins (Fig. 2). The mutant EFEMP1 protein appeared to form extracellular aggregates that extend along the abnormal ECM made by ARPE-19-*EFEMP1*$^{R345W/R345W}$

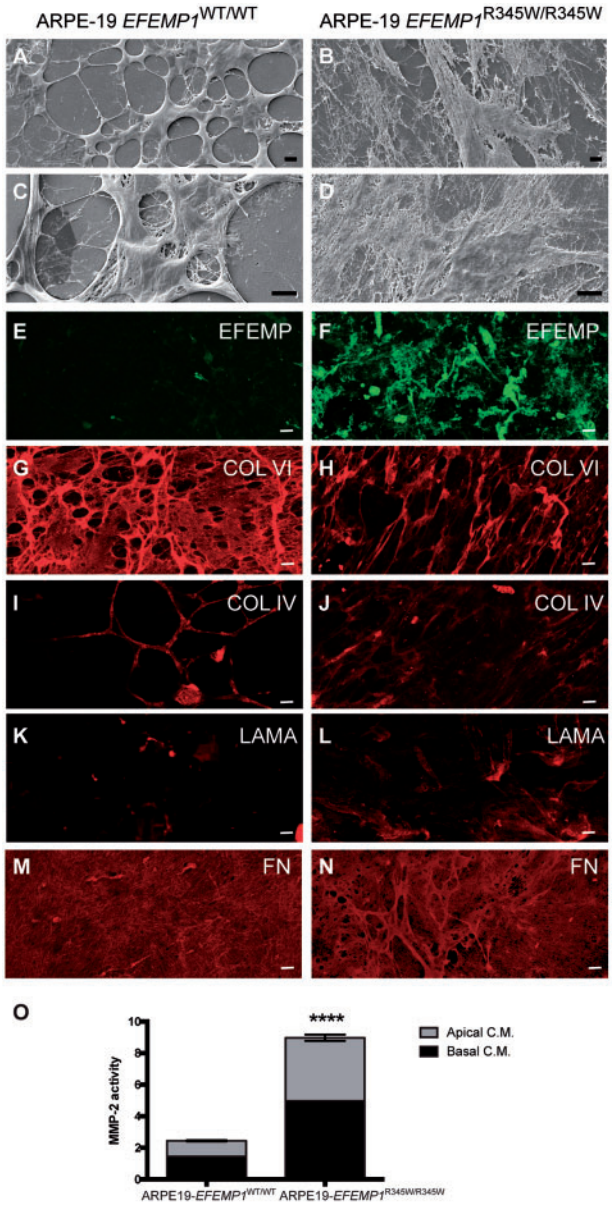

Figure 2. Edited ARPE-19-*EFEMP1*$^{R345/R345W}$ cells make abnormal ECM. Decellularized transwells of ARPE-19 wild-type (left panels) and ARPE-19-*EFEMP1*$^{R345/R345W}$ (right panels) cultures after 4 weeks. SEM images show normal ECM (**A** and **C**) versus abnormal ECM (**B** and **D**) made by wild-type and mutant cells respectively. Immunostaining with antibodies for EFEMP1 (**E** and **F**), Col VI (**G** and **H**), Col IV (**I** and **J**), laminin (**K** and **L**) and fibronectin (**M** and **N**) show the abnormal structure of the ECM. Scale bars (A–N): 10 μm. (**O**) Relative MMP-2 activity measured by zymography in apical and basal conditioned media of ARPE-19-*EFEMP1*$^{WT/WT}$ and ARPE-19-*EFEMP1*$^{R345/R345W}$ cells (data represented as mean ±SD; *t*-test; ****$P < 0.0001$).

(Fig. 2E), similar to what we found in primary RPE from *Efemp1*$^{R345W/R345W}$ mutant mice (30). In contrast, EFEMP1 is barely visible in the ECM made by wild-type ARPE-19 cells (Fig. 2F). Collagen VI labeling in the wild-type ECM is visualized as a continuous network of fibers with some thickened and localized areas (Fig. 2G), while the mutant ECM presents a disorganized network of stretched fibers (Fig. 2H). Collagen IV labeling shows a similar pattern of that collagen VI, with less intense staining (Fig. 2I and J). Weak laminin staining appears to localize in areas where ECM fibers converge (Fig. 2K), and is more extended in the mutant ECM (Fig. 2L). Fibronectin labeling (Fig. 2M) reveals an open network of fibers in the wild-type ECM, while in the mutant ECM the fibronectin network appears to be thicker, with more than one layer of fibers (Fig. 2N).

Zymography analyses demonstrated that MMP-2 activity was significantly increased in conditioned media from ARPE-19-*EFEMP1*$^{R345W/R345W}$ cells compared with wild-type (*t*-test, $P < 0.0001$), which indicates that the ECM turnover is also affected by the p.R345W mutation (Fig. 2O).

ECM made by ARPE-19-EFEMP1$^{R345W/R345W}$ cells binds active complement components

The presence of active complement components anchored to the ECM made by ARPE-19-*EFEMP1*$^{WT/WT}$ and ARPE-19-*EFEMP1*$^{R345W/R345W}$ cells was demonstrated by immunostaining of the exposed ECM after decellularization. Increased deposition of C3b on the abnormal ECM was demonstrated with an antibody that binds C3b once it has been cleaved; but it does not recognize full length C3 (ANOVA, $P = 0.0172$) (Fig. 3) (48). This antibody also binds C3(H2O) generated by hydrolysis of C3 via tick-over. Co-immunostaining with CFH antibodies showed that both C3b/C3(H2O) and CFH are deposited on the abnormal ECM and overlay most of the surface of the abnormal ECM, compared with the wild-type ECM, where the protein deposition is discreet (Fig. 3E and F). We did not detect C3a in conditioned media from edited ARPE-19 wild-type or ARPE-19-*EFEMP1*$^{R345W/R345W}$ cells.

Normal primary RPE cells grown on abnormal ECM make basal deposits similar to basal laminar deposits in AMD patients

To determine if the abnormal ECM made by the ARPE-19-*EFEMP1*$^{R345W/R345W}$ cells can affect the viability and function of normal RPE cells, we isolated primary hfRPE cells and seeded them on the exposed ECM made by ARPE-19-*EFEMP1*$^{WT/WT}$ and ARPE-19-*EFEMP1*$^{R345W/R345W}$ cells on transwells. hfRPE cells were cultured for 2 weeks in the absence of serum. Although the morphology of the cells in both cultures was similar (Fig. 4A–C), transepithelial electrical resistance (TER) after 2 weeks was slightly but significantly lower in cultures grown on abnormal ECM compared with wild-type or commercial ECM (*t*-test, $P = 0.0123$) (Fig. 4D).

To study the formation of basal deposits by normal hfRPE cells grown on abnormal ECM, transwells were decellularized after 2 weeks of hfRPE culture, and the exposed ECM was fixed for immunostaining and SEM. SEM images demonstrated that hfRPE cells grown on normal ECM make typical ECM that covers the insert uniformly (Fig. 5A and C). In contrast, the same hfRPE cells grown on abnormal ECM make thick basal deposits that coat the surface of the transwell as a network of fibers with numerous thickened areas over the original abnormal ECM (Fig. 5B and D).

To test if the deposits made by the hfRPE cells were similar to the basal laminar deposits found in AMD patients, immunostaining with antibodies for the main components of the latter (EFEMP1, collagen VI, collagen IV, laminin and fibronectin) was performed on the exposed ECM and deposits (Fig. 5). EFEMP1 was not detected in normal ECM (Fig. 5E), but was clearly present in the basal deposits (Fig. 5F). While normal ECM showed a discreet labeling for collagen VI (Fig. 5G), collagen VI is a major component of the abnormal ECM (Fig. 5H). Collagen IV is present in both the normal and abnormal ECM, although with

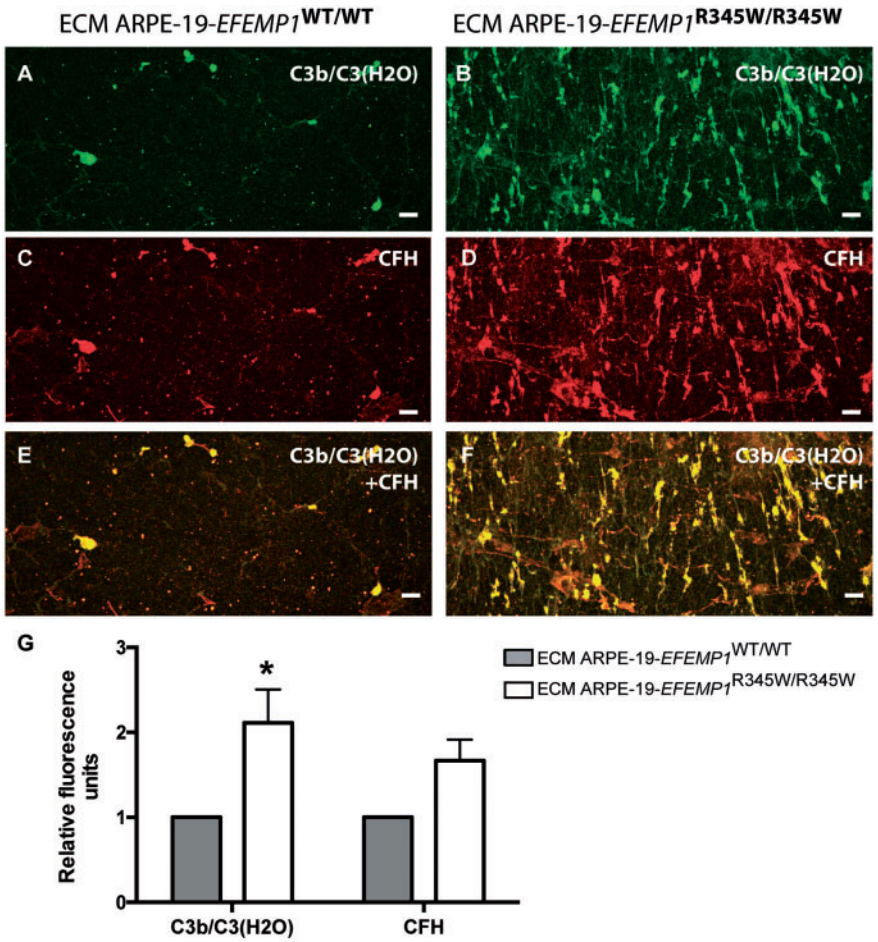

Figure 3. Abnormal ECM anchors C3b and CFH. Decellularized transwells of ARPE-19 wild-type (left panels) and ARPE-19-*EFEMP1*$^{R345/R345W}$ (right panels) cultures. Exposed ECM immunostained with antibodies for (**A** and **B**) C3b/C3(H2O) and (**C** and **D**) CFH. (**E** and **F**) Co-staining for C3b/C3(H2O) and CFH. Scale bars 50 μm. (**G**) Average quantification of C3b/C3(H2O) and CFH fluorescent labeling comparing exposed ECMs (data represented as mean ± SD. ANOVA, $^{*}P < 0.05$).

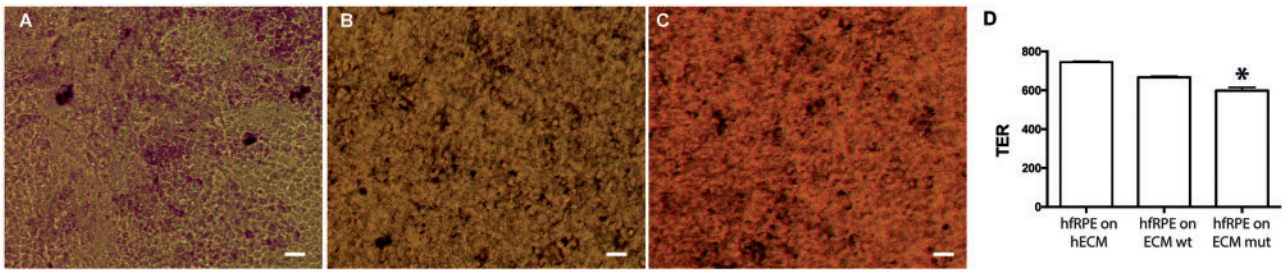

Figure 4. HfRPE grown on normal versus abnormal ECM. Brightfield microscopy of hfRPE cells grown for 2 weeks on (**A**) commercial human ECM, ECM made by (**B**) ARPE-19 wild-type or (**C**) ARPE-19-*EFEMP1*$^{R345/R345W}$ cells. Scale bars 10 μm. (**D**) TER measured in hfRPE cell cultured on human ECM, ECM made by ARPE-19 wild-type or ARPE-19-*EFEMP1*$^{R345/R345W}$ cells for 2 weeks ($n = 3$ cultures/ECM type. *t*-test, $^{*}P < 0.05$).

different patterns of staining (Fig. 5I and J). Laminin had diffuse labeling in both normal ECM and deposits, with apparently stronger staining in the deposits (Fig. 5K and L). Less fibronectin labeling was detected in the deposits with a disrupted staining pattern compared with normal ECM (Fig. 5M and N).

Impaired ECM turnover in RPE cultures with basal deposits

Aging is associated with thickening of BrM, which is thought to be owing to impaired regulation of ECM synthesis and turnover (3–7). Turnover of BrM, specially the degradation of collagen IV, is controlled by MMP-2 produced by the RPE (8). To evaluate the impact of alterations in ECM turnover in the production of abnormal ECM by hfRPE, we measured MMP-2 activity in the apical and basal media of hfRPE cells grown on normal and abnormal ECM, produced by ARPE-19-*EFEMP1*$^{WT/WT}$ and ARPE-19-*EFEMP1*$^{R345W/R345W}$ cells, respectively. Increased MMP-2 activity was demonstrated in basal but not apical conditioned media of hfRPE cells grown on abnormal ECM (Fig. 6A) (ANOVA, $P = 0.0086$). The higher levels of MMP-2 only in basal media appear to be a consequence of posttranslational activation of

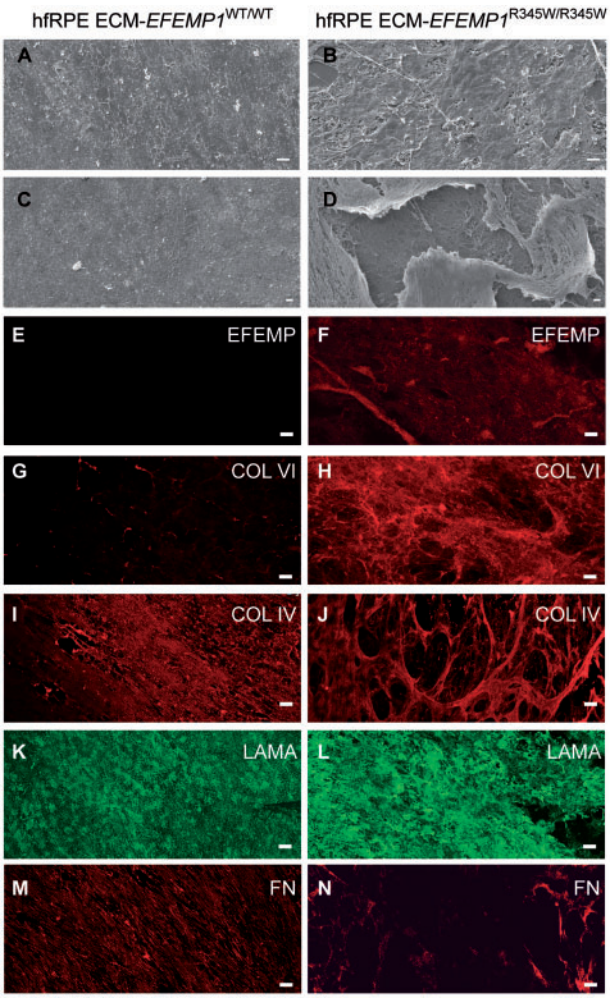

Figure 5. HfRPE cells grown on abnormal ECM make basal deposits. (**A** and **C**) hfRPE cells grown for 2 weeks on ECM made by ARPE-19 wild-type cells were decellularized and imaged by SEM. Images show the remaining exposed normal ECM made by hfRPE cells. (**B** and **D**) hfRPE cells grown for 2 weeks on ECM made by ARPE-19-*EFEMP1*$^{R345/R345W}$ cells were decellularized and imaged by SEM. Images show the remaining thick basal deposits made by hfRPE cells. In some of these areas, the outer layer of the deposits is lifted and a network of crosslinking ECM fibers can be observed underneath. Immunostaining of the exposed ECM and deposits with antibodies for EFEMP1 (**E** and **F**), Col VI (**G** and **H**), Col IV (**I** and **J**), laminin (**K** and **L**) and fibronectin (**M** and **N**). Immunolabeling of deposits revealed a very strong signal for collagen VI, and the distribution of both collagen VI and IV was heterogeneous and disposed as a tridimensional network of crosslinked bundles of collagen fibers. The data show that the composition of the deposits made by hfRPE grown on abnormal ECM is similar to the composition basal deposits in AMD patients. Scale bars A–D: 10 μm, E–N: 50 μm.

MMP-2 by the abnormal ECM underneath the cells, since the level of MMP-2 mRNA did not change between conditions (*t*-test, $P = 0.1769$) (Fig. 6B).

Abnormal ECM triggers local activation of the alternative complement pathway by normal RPE cells via tick-over

We next asked if the abnormal basal laminar deposit material produced by hfRPE cells grown on abnormal ECM was associated with increased local activation of complement via the tick-over process, resulting in increased C3 deposition on the abnormal ECM. Immunostaining of the decellularized ECM generated by hfRPE grown for 2 weeks on normal (made by ARPE-19-*EFEMP1*$^{WT/WT}$) versus abnormal (made by ARPE-19-*EFEMP1*$^{R345W/R345W}$) ECM in the absence of serum with antibodies for C3b/C3(H2O) demonstrated increased deposition of activated C3 on the abnormal basal deposit material compared with the normal ECM (*t*-test, $P = 0.0279$) (Fig. 7A and B). CFH was also detected in areas of strong staining for C3b/C3(H2O) (Fig. 7C–F).

Unlike classical and lectin pathways, which need the presence of microbial pathogens, alternative complement pathway can be activated via tick-over by deposition of C3b on foreign structures. We tested the hypothesis that induction of the tick-over mechanism via C3b deposition can cause chronic activation of the alternative complement pathway by hfRPE grown on the abnormal ECM. For that, we measured complement activation in conditioned media of hfRPE cells grown for 2 weeks on normal versus abnormal ECM in the absence of serum. Enzyme-linked immunosorbent assay (ELISA) analyses demonstrated a substantial increase of C3a, CFH and CFB in basal conditioned media of hfRPE cells grown on abnormal ECM (Fig. 7G–I) (ANOVA, $P = 0.0096$, $P = 0.0219$ and $P = 0.0077$, respectively). mRNA levels of complement components did not show any change in hfRPE cells grown on different ECMs (Fig. 7J).

Alterations in BrM of patients with AMD cause abnormal ECM turnover and complement activation by normal RPE cells

We hypothesize that increased activation of the complement system by the RPE in response to abnormal ECM is a shared mechanism in *EFEMP1*-associated macular degeneration and AMD. To test this hypothesis, we evaluated the responses of normal hfRPE growth on BrM obtained from human eyes with and without AMD. For these studies, we collected human eyes from age matched donors with and without AMD (ages = 85 ± 1 years). Four normal eyes and four eyes with AMD were used. To evaluate the status of BrM in these eyes, BrM–choroid–sclera explants were evaluated by SEM and immunostaining with antibodies to Collagen IV, which is a major component of the basal lamina in BrM (5,49). SEM images demonstrated that BrM of AMD patients had an irregular pattern, where collagen fibers form a network with hexagonal mosaic shape and spotted abnormal structures that resemble drusen (Fig. 8A and B). Collagen IV was present in an irregular pattern in the AMD eyes, compared with more homogeneous labeling in control explants (Fig. 8C and D).

We next evaluated the response of hfRPE cells grown on the BrM from the normal and AMD eyes. For these studies, 6 mm BrM–choroid–sclera explants were freshly prepared, and normal hfRPE cells from the same fetus donor were seeded at a density of 3164 cells/mm^2 (~100 000 cells/explant) in RPE medium with 5% fetal bovine serum (FBS). After 48 h, media was changed and hfRPE cells were cultured on explants in RPE medium for two additional weeks in the absence of serum. The viability of the RPE cells grown on explants was verified by transmission electron microscopy after 2 weeks (Supplementary Material, Fig. S2). MMP-2 activity in conditioned media was significantly increased in cultures grown on AMD explants compared with controls, indicating that the ECM turnover is also impaired by the BrM of AMD donors (*t*-test, $P = 0.0020$) (Fig. 8E). Increased levels of C3a were detected in the conditioned media from hfRPE cells grown on explants with AMD but not media from cells grown on control explants (Fig. 8F) (ANOVA, $P < 0.0001$). These data confirm that the abnormal ECM in the AMD BrM is

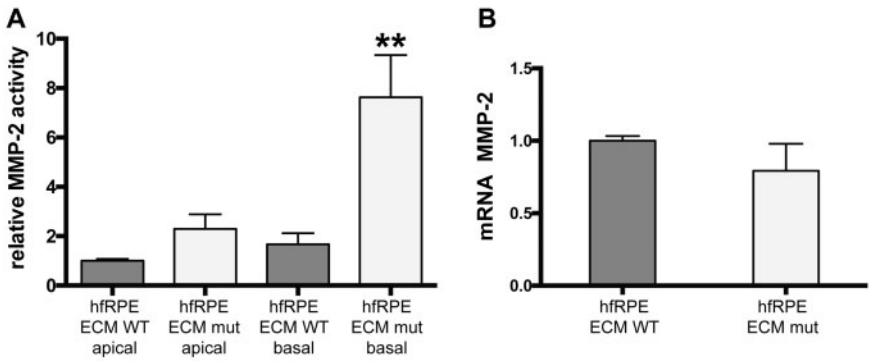

Figure 6. Abnormal ECM alters the ECM turnover. (**A**) MMP-2 activity measured by zymography in apical and basal conditioned media of hfRPE cells cultured on normal (wt) or abnormal (mut) ECM made by ARPE-19-*EFEMP1*$^{R345/R345W}$. (**B**) mRNA levels of MMP-2 measured in the same cultures, normalized to GAPDH (data represented as mean ± SEM; *t*-test, $^{**}P < 0.01$; $n = 4$/ECM type).

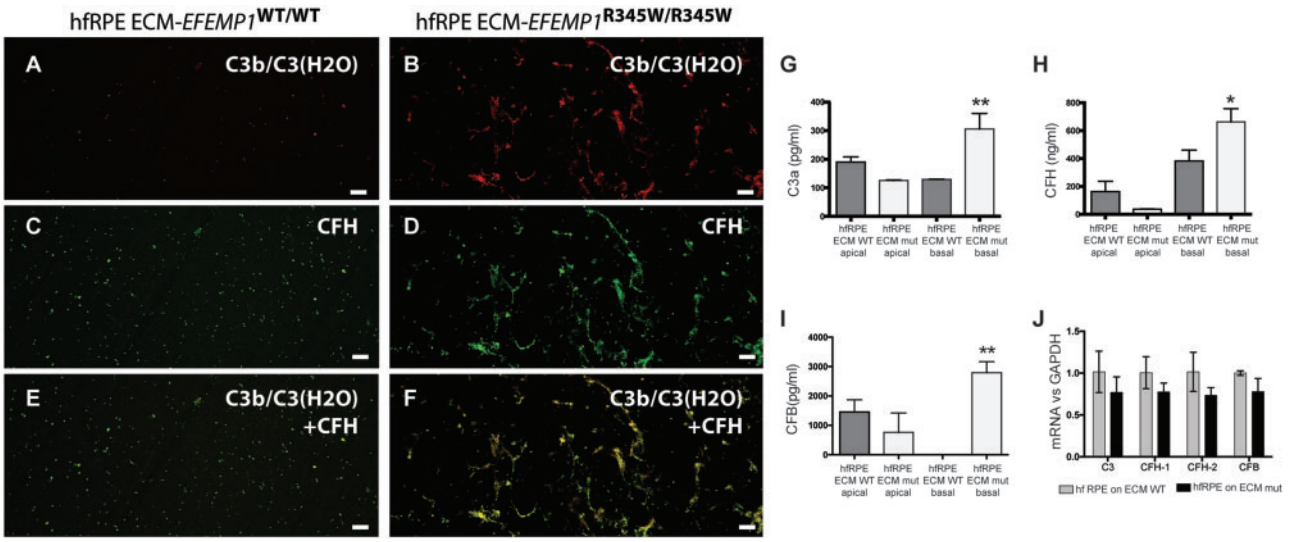

Figure 7. Abnormal ECM causes complement activation by normal hfRPE cells. hfRPE cultures grown on ECM made by ARPE-19 wild-type or ARPE-19-*EFEMP1*$^{R345/R345W}$ were decellularized and immunostained with antibodies for (**A** and **B**) C3b/C3(H2O), (**C** and **D**) CFH or (**E** and **F**) both C3b/C3(H2O) and CFH. Scale bars: 50μm. (**G**) C3a, (**H**) CFH and (**I**) CFB measured by ELISA in apical and basal conditioned media of hfRPE cells grown on ECM made by ARPE-19 wild-type (ECM WT) or ARPE-19-*EFEMP1*$^{R345/R345W}$ (ECM mut) in the absence of serum (data represented as mean ± SD. ANOVA, $n = 4$ per type, $^{*}P < 0.005$, $^{**}P < 0.001$). (**J**) mRNA levels of complement components from the alternative pathway measured in hfRPE cells grown on normal (gray) or abnormal (black) ECM made by wild-type or mutant ARPE-19 cells, respectively.

sufficient to cause local activation of complement system by normal RPE cells.

Discussion

The results reported here demonstrate that abnormalities in the ECM, including those caused by the p.R345W mutation in EFEMP1 or aging and other risk factors in AMD, are sufficient to cause activation of complement system and formation of basal deposits by normal RPE cells. Like RPE cells from *Efemp1* mutant mice, genome edited ARPE-19-*EFEMP1*$^{R345W/R345W}$ cells make abnormal ECM *in vitro*, which is associated with increased complement activation as indicated by increased levels of C3b in the ECM. The abnormal ECM made by the ARPE-19-*EFEMP1*$^{R345W/R345W}$ cells stimulated activation of C3 and production of basal deposits by normal hfRPE cells. Of particular note, similar responses were also observed when normal hfRPE cells were cultured on BrM from patients with AMD, suggesting that stimulation of complement activation by abnormal ECM is a shared step in the early pathogenesis of both inherited and AMDs. Further, impaired remodeling of the ECM produced by RPE cells also appears to be a shared feature of early disease between inherited and AMDs, as increased MMP-2 activity was observed in the basal media of hfRPE cells cultured on the ECM produced by ARPE-19-*EFEMP1*$^{R345W/R345W}$ cells and on BrM from AMD patients. These data provide insight into the early pathogenesis of macular degenerations, and suggest that alterations in complement activation occur earlier in disease than previously described.

Our previous studies using a mouse model of the early-onset *EFEMP1*-associated macular degeneration demonstrated that the formation of sub-RPE deposits *in vitro* occurs in response to local activation of complement system by the RPE (30). However, we did not know how abnormalities in the ECM can cause complement activation or which complement pathway(s) were involved. Also, the fact that *EFEMP1*-associated macular degeneration is an ultra-rare disease, makes it difficult to find donors to reproduce those studies using human primary cells. Here, the data show that abnormal ECM made by ARPE-19-*EFEMP1*$^{R345W/R345W}$ cells has changes in structure and composition similar to those observed in the aged BrM of AMD

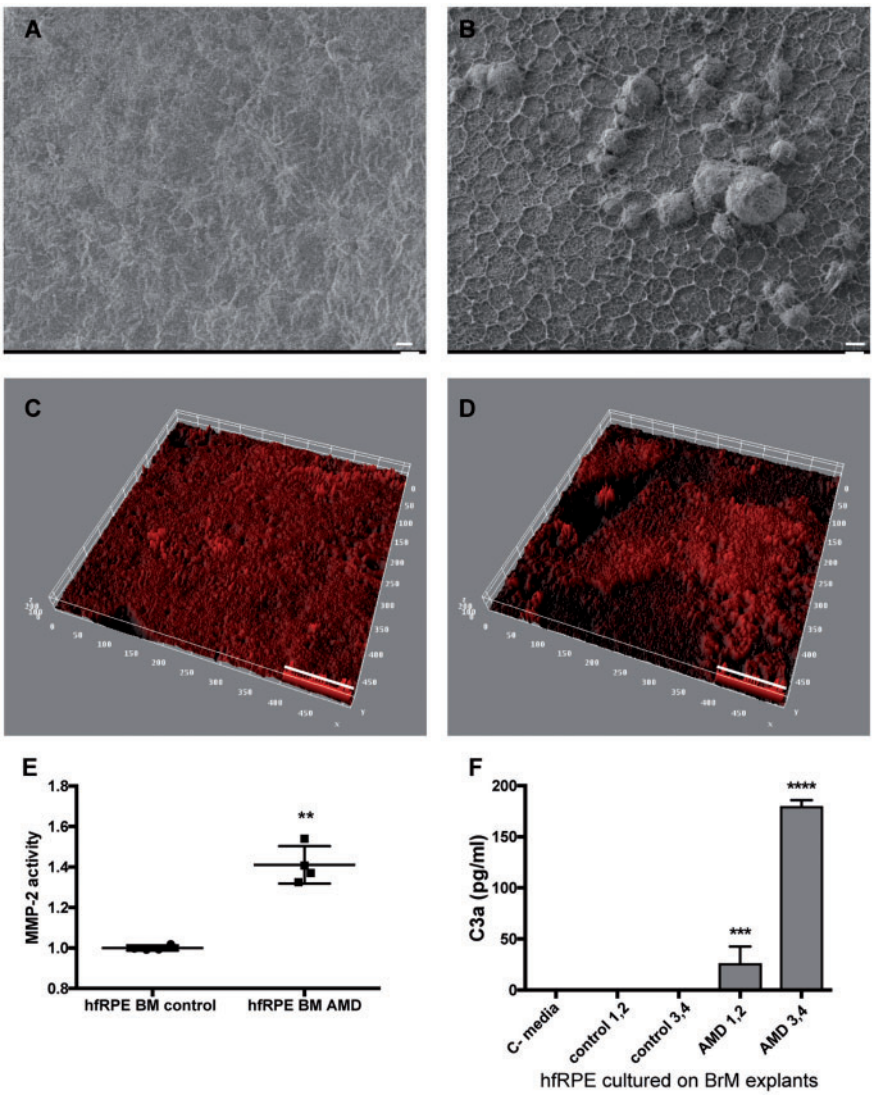

Figure 8. BrM with AMD alters ECM turnover and causes complement activation by normal hfRPE cells. SEM of BrM from (**A**) normal and (**B**) AMD donors. Thick ECM network and drusen-like deposits are visible in the BrM of AMD donors. Representative 3D reconstruction of BrM explants from (**C**) normal and (**D**) AMD donors immunostained for collagen IV, and imaged by confocal microscope. Quantification of (**C**) MMP-2 activity and (**D**) C3a in conditioned media from hfRPE cells cultured on BrM–choroid–sclera explants from donors without AMD (control 1–4) and with AMD (AMD 1–4). C-media: no cells (data represented as mean ± SD. $n = 4$ explants/type. ANOVA, $^{****}P < 0.0001$, $^{***}P < 0.001$, $^{**}P < 0.01$). Scale bars: (A, B)=10 μm, (C, D)=50 μm.

patients (5,50). This abnormal ECM binds active complement components, as demonstrated by increased deposition of C3 and CFH. However, we did not detect C3a in the conditioned media from these cells, perhaps because the concentration was too low. The abnormal ECM observed may be owing to impaired ECM turnover, since increased MMP-2 activity was present in conditioned media from ARPE-19-*EFEMP1*$^{R345W/R345W}$ cells. However, in the mouse model, we found decreased MMP-2 activity in *Efemp1*$^{R345W/R345W}$ RPE cultures compared with wild-type (30). We believe that the increased MMP-2 activity in ARPE-19 mutant cultures may be due in part to decreased inhibition of MMP activity by TIMP-3 in the basal media. TIMP-3 interacts with EFEMP1 by the domain that contains the R345W mutation (43). Moreover, while the mutant EFEMP1 protein seems to be equally secreted by wild-type and mutant mouse RPE cells, human cell lines carrying the mutation R345W in EFEMP1 have been reported to secrete less amount of EFEMP1 to the media (51), which could result in lesser inhibition of MMP-2 by TIMP-3 in ARPE-19 mutant compared with wild-type cultures.

We tested the hypothesis that changes in the structure and composition of BrM in early AMD affect the function of RPE and generate inflammation. Precise genome editing of the human ARPE-19 cell line carrying the *EFEMP1*$^{R345W/R345W}$ mutation allowed development of a model that recapitulates the RPE/BrM pathology at early stage of AMD. SEM and immunostaining analyses demonstrated that normal hfRPE cells grown on abnormal ECM produced by ARPE-19-*EFEMP1*$^{R345W/R345W}$ cells make thick basal deposits with increased collagens VI and IV, in addition to a distinct pattern for ECM components of basal laminar deposits. The abnormal deposition of basement membrane material underneath the RPE is also a characteristic feature of early stage AMD (5,41,47,50,52,53). In addition, explants of BrM with AMD also showed increased deposition of ECM and collagen IV. Accordingly, our model is an effective tool to study the mechanisms underlying the formation of basal deposits, which

is a hallmark of early AMD. Moreover, it demonstrates that modeling some aspects of complex diseases using Mendelian diseases is feasible with CRISPR–Cas9-mediated genome editing, the efficiency of which can be improved by the addition of the DNA ligase IV inhibitor, SCR7 (54).

It is currently accepted that MMPs are specific proteolytic enzymes rather than mere ECM degraders. In this way, MMPs are key for the homeostasis of the extracellular environment and regulation of innate immunity (55). Aberrant ECM expression and remodeling can trigger the activation of immune cells in chronically inflamed tissues (10). In the case of BrM, MMP-2 produced by the RPE is crucial for the remodeling of the basement membrane, which increment with age results in BrM thickening, altered ECM turnover and inflammation (5,6,8,9,56). The increased MMP-2 observed in hfRPE cultures grown on abnormal ECM indicates that the ECM turnover and remodeling is impaired, which causes further abnormal deposition of ECM proteins. It is also probable that the RPE secretes MMP-2 in an attempt to recover ECM homeostasis by eliminating the collagen accumulated underneath. In the context of other human inflammatory diseases, proteolysis of collagen results in bioactive fragments that promote the local accumulation of debris, cytokines, chemokines and other ECM proteolytic fragments and regulators (10–12). We think that the accumulation of these fragments could explain, in part, the formation of basal deposits (4,6). For instance, the abnormal accumulation of these substances in the ECM along with the abnormal structure of the interface between the RPE and BrM may lead to complement activation. Our data determined that abnormal ECM stimulates the activation of complement by hfRPE cells as shown by increased C3a, CFB and CFH in the basal media. HfRPE cells also show increased complement activation, as demonstrated by C3a in media, following growth on BrM from AMD compared with control eyes. Hence, the mechanism of abnormal ECM causing increased complement activation is also shared between *EFEMP1*-associated macular degeneration and AMD.

In contrast to specific interactions that initiate classical and lectin pathway activation by pathogens, the alternative pathway can be autoactivated via tick-over by covalent attachment of C3b to nearby surfaces (57). Although the tick-over is a basal process, it can be actively induced when C3(H2O) is deposited on abnormal ECM (34–36). Specifically, C3(H2O) has great affinity to bind collagen IV and laminin (36), which are major components of the abnormal ECM and basal deposits made by the mutant RPE cells in our model. We believe that C3(H2O)-convertase stabilizes on the abnormal ECM, evading CFH inhibition, which results in binding of CFB and further chronic activation of the alternative complement pathway and increased CFH and C3a in media (33,37,38). Our hypothesis is supported by the fact that only hfRPE cells seeded on abnormal ECM or BrM with AMD in the absence of pathogens showed increased C3a, while no complement activation was detected when the same cells were grown on normal ECM or BrM without AMD. Taken together, these data suggest that the primary activation of the complement system in the deposits occurs via tick-over and posterior amplification of the alternative pathway. However, additional analyses are needed to corroborate this supposition.

To our knowledge, this is the first demonstration that abnormal matrix can initiate the local activation of the alternative complement pathway as one of the early steps in the pathogenesis of AMD. The process has similarities with other diseases such as fibrosis, arthritis, kidney disease, Alzheimer's disease and cancer, in which the excessive deposition of ECM triggers inflammatory responses (58–62). However, other factors such as genetic variants that alter the responsiveness of the complement system are needed to initiate disease in AMD (15). These data help define the earliest stages in macular degeneration disease pathogenesis. They also confirm the importance of complement system in dry AMD, and most importantly, they suggest that alterations in complement activity participate in disease earlier than previously described (13,14,63). As a novelty, they suggest that the local cleavage of C3 via convertase-independent mechanisms can be a new therapeutic target for early AMD. Further, our model can be used to test different treatments *in vitro*, as well as to better understand the mechanisms that lead from BrM thickening to basal deposit formation and disease progression in AMD.

In conclusion, new drugs addressing the specific steps involved in the RPE, such as the local cleavage of C3 via tick-over process, may be efficient at early stages of AMD. The efficacy of therapies for the treatment of early AMD might be also improved using regulators of the ECM synthesis and turnover, a target that has shown to be key in other human diseases such as cancer, fibrosis and cardiovascular disease (64–66). Finally, drugs applied locally could be an improved approach for patients with drusen, and could stop or at least delay the progression of the disease to legal blindness without compromising the whole immune system or vital biological processes.

Materials and Methods

CRISPR/Cas9 genome editing

Single guide RNA (sgRNA) design: ARPE-19 cells (ATCC® CRL-2302™, Manassas, VA, USA) were edited using the CRISPR technology as previously described (44,45). The single guide sgRNA target sequence (GACCACAAATGAATGCCGGG) was designed with the tool http://crispr.mit.edu/, with a score of 82. All potential off-targets have at least two mismatches and a maximum score of 2.2. Potential off-targets with a score >0.2 were ruled out by PCR followed by Sanger Sequencing. The sgRNA was cloned onto the vector pSpCas9(BB)-2A-GFP (PX458) (a gift from Feng Zhang, Addgene plasmid no. 48138) using the BbsI site to be expressed under the U6 promoter.

Transfection of ARPE-19 cells. ARPE-19 cells were transfected with the Amaxa nucleofector kit V (Lonza, Portsmouth, NH, USA) following the manufacturer's instructions. Five micrograms of plasmid DNA was co-transfected with 5μl of 10μM ssODN donor (5′ T CTC TGG TGT TAG AAT GTA GGG ATC TTG ACA AGG ATT TCG TGG ATA ACA ACG GAA GCC GCC ATG ATA ATT CCA ACA CAT TTC ATC TTC CCA GCA TTC ATT TGT GGT CTC ACA CTC ATT TAT GTC CGT AGA TAT GTA GGG TCA AAG AGT TTA CTA ACT AAA CTA ATG AAC TGA TCT AAT TAA 3′) per 10^6 cells in a 10 cm dish. Silent mutation was introduced to the PAM sequence in order to avoid cuts in the ssODN (Fig. 1). After transfection, the cells were cultured in DMEM: F12 + 10% FBS in the presence of 1μM of SCR7 (ApexBio, Houston, TX, USA), a DNA ligase IV inhibitor (54,67), for 48 h.

Cutting efficiency was tested using the SURVEYOR assay 48 h post-transfection as previously described (45). Briefly, cells were lysed and DNA was extracted using 10μl of the QuickExtract DNA extraction solution (Epicentre, Madison, WI, USA) per 96-well, and 1μl was amplified using the primers F: 5' TCCCCC TGGCAAAATTACCC 3' and R: 5' AGTTGTGGCCTGTATCTGGA 3' following the conditions published by Ran et al. (45). Four hundred nanograms of PCR product were used to form the heteroduplex, later digested with 2ud of T7 Endonuclease I

(New England Biolabs, Ipswich, MA, USA) for 30 min at 37 °C. Fragments were resolved in a 2.5% agarose gel.

Isolation of clonal cells was performed by limit dilution as previously described (45). Although the vector pSpCas9(BB)-2A-GFP (PX458) has GFP and it can be sorted by fluorescence, pilot experiments showed that recovery efficiency for ARPE-19 was very low after sorting compared with limit dilution. Thus, the GFP signal was only used to estimate the rate of transfection under fluorescent microscope (>90%). Forty-eight-hour post-transfection cells were diluted to 1 cell/well in 96-well plates and expanded until 60% confluence was reached (around 4 weeks). Then two replica plates were prepared, one to keep cells growing in incubator and one to analyze the genotype of the edited clones (45). After 1 week, wells with no clones or more than one clone were discarded.

Genotype of edited clones by PCR-RFLP: DNA was extracted from replica plate using the QuickExtract DNA extraction solution (Epicentre, Madison, WI, USA) as previously described (45). The change C>T c.1034 in the *EFEMP1* gene creates a new restriction site for the *BseYI* enzyme, which allows for the rapid screening of positive edited clones by PCR-RFLP before Sanger sequencing (Fig. 1B). PCR fragments amplified using the primers F: 5′ TGT CCCTGATGACAAGAACTGG3′ and R: 5′ CTCGGCACATGGCAT TTGAG 3′ (amplicon size 569 bp) were digested with *BseYI*, generating two fragments of 364 and 215 bp when the recombination had taken place. The positive C>T c.1034 knock-in clones were sequenced by Sanger to rule out unwanted indels and off-targets. The counterpart replica wells maintained in culture were expanded in DMEM: F12 + 10% FBS and used for subsequent experiments or cryopreserved.

Hemizygous samples were genotyped by cloning above-mentioned PCR fragments with the TA Cloning® Kit, with pCR™2.1 Vector and One Shot® TOP10 Chemically Competent *E. coli* (Invitrogen/Thermo Fisher Scientific, Waltham, MA) following the manufacturer's instructions. Minipreps were performed using Zyppy™ Plasmid Miniprep Kit (Zymo Research, Irvine, CA, USA) and sequenced by SANGER.

Generation of ECM by ARPE-19-EFEMP1$^{WT/WT}$ and ARPE-19-EFEMP1$^{R345W/R345W}$ cells

Selected clones of ARPE-19 cells carrying none or two copies of the mutation C>T c.1034 were seeded on 12-mm polyester transwells (Corning, NY, USA) at a density of 4×10^4 cells per transwell in RPE media +10% FBS per triplicate. FBS was removed after 24 h and cells were further grown in RPE media in the absence of serum. After 4 weeks, transwells were decellularized by incubating them with sterile 0.5% Triton X-100 + 20 mM NH_4OH in PBS (1.5 ml was added to the bottom chamber and 0.5 ml to the apical chamber) for 5 min at 37 °C, followed by several washes with sterile PBS. hfRPE cells were seeded immediately on the exposed ECM or inserts were fixed for subsequent analyses.

HfRPE isolation and culture

Eyes from 16 to 20 weeks of gestation fetuses were obtained from Advanced Bioscience Resources (Alameda, CA, USA) placed in RPMI on ice, and delivered by an overnight priority delivery service. All tissues were used less than 24 h after enucleation. Primary hfRPE cells were collected as previously described with minor modifications (46,68). Briefly, upon reception eyes were rinsed in antibiotic–antimycotic solution for 5 min at RT. Connective tissue was removed and the anterior portion of the eye, cornea, iris and vitreous were also removed. Eyecups were incubated in Dispase I solution (2 U/ml in RPE media + 5% FBS) for 25 min at 37 °C. Neural retina was then removed and the RPE sheet was peeled off with fine forceps and incubated in 0.25% Trypsin+ 0.02% EDTA for 10 min at 37 °C in a water bath. After centrifugation, cells from one eye were resuspended in RPE media + 15% FBS and seeded on a total of six transwells, three decellularized transwells containing ECM made by ARPE-19-*EFEMP1*$^{WT/WT}$ and three containing ECM made by ARPE-19-*EFEMP1*$^{R345W/R345W}$. Confluence after 24 h was around 30%. FBS was removed from the media after 72 h. After 2 weeks, transwells were decellularized as previously described and fixed in 4% paraformaldehyde (PFA) for subsequent analyses.

RPE media

RPE media was prepared as previously described (46,69). N1 Medium Supplement 1/100 (vol/vol), glutamine 1/100 (vol/vol), penicillin-streptomycin 1/100 (vol/vol) and non-essential amino acid solution 1/100 (vol/vol), hydrocortisone (20 μg/l), taurine (250 mg/l) and triiodo-thyronin (0.013 μg/l) in alpha MEM (46) + 5% heat inactivated FBS (Hyclone, Logan, UT, USA) or without FBS.

Transepithelial electrical resistance

Transepithelial electrical resistance (TER) of the RPE cultures was measured using an epithelial voltohmmeter (46,70).

Preparation of BrM explants

BrM explants were obtained from human donors through the National Disease Research Interchange (Philadelphia, PA, USA). Eyes from two donors diagnosed with AMD and two normal donors (ages 85 ± 1) were enucleated within 10 h postmortem and shipped to our facility within 24 h in a sterile container in DMEM on ice. BrM macular explants were prepared upon receipt as previously described (71). Briefly, eyes were washed in 10% povidone iodine for 10 min two times at RT, then rinsed with DMEM containing antibiotics. A circular incision was made below the ora serrata to remove cornea, lens, iris, vitreous and neural retina. RPE cells were removed by incubation with sterile 20 mM NH_4OH + 0.5% Triton in PBS for 20 min at 37°C. RPE cells were then flowed out with PBS 1× using a p1000 micropipette. Eyecups were inspected under dissection microscope to ensure the complete removal of RPE cells. A 6-mm explants containing BrM–choroid–sclera were performed with a trephine, and placed onto 96-well plates in PBS. Explants were fixed in 4% PFA for 10 min for subsequent analyses by immunostaining and SEM, or used fresh to seed hfRPE cells at a density of 3164 cells/mm^2 (~100 000 cells/explant). Cells were grown in RPE media with 5% of FBS for 48 h and then in the absence of serum for two additional weeks with three changes of media.

Immunostaining

Transwell inserts containing exposed ECM after decellularization of cultures were rinsed in PBS, fixed for 10 min in 4% PFA in PBS followed by fixation in 1% glutaraldehyde for 30 min at room temperature. Then inserts were cut-off with a razor blade and stored upside in PBS at 4 °C pending immunohistochemical analyses. Inserts were cut into small pieces and blocked with 1% BSA for 30 min at RT. Primary antibodies were incubated overnight at 4 °C. Secondary antibodies labeled with Alexa-488 or Alexa-555 (Life Technologies, Grand Island, NY, USA) were incubated for 1 h at RT. Sections were mounted with

Fluoromount G (Electron Microscopy Sciences, Hatfield, PA, USA) and visualized by TCS SP5 II confocal laser scanning microscope (Leica). Controls were incubated only with secondary antibody. Primary antibodies used were: Col IV (AB6586, Abcam, Cambridge, MA, USA), Col VI (AB6588), LAM (AB11575), FN (AB2413), EFEMP1 (SC33722, Santa Cruz Biotechnology, Santa Cruz, CA, USA) C3b/C3(H2O) (HM2286, Hycult Biotech, Plymouth Meeting, PA, USA), CFH (AB53800).

For the immunostaining of BrM, explants of BrM–choroid–sclera were incubated with antibodies as described above in 96-well plates. After incubation with the secondary antibody, explants were incubated with 0.1% Sudan Black B in 70% ethanol for 5 min at RT to remove autofluorescence, and then washed with 70% ethanol to eliminate the excess of dye. BrM–choroid was then peeled off and flat mounted (oriented with the BrM side up) with Fluoromount G on a slide. Samples were visualized by TCS SP5 II confocal laser scanning microscope (Leica).

Quantification of the fluorescent signal

Images were converted to binary format with ImageJ (72). The integrated intensity was measured.

Tridimensional reconstruction of BrM explants

z-Stack images were taken every 0.5 microns, then 3D surface was reconstructed and plotted using ImageJ (72).

Scanning electron microscopy

Transwell inserts containing exposed ECM after decellularization of cultures and BrM explants were fixed as previously described. Samples were washed in PBS, hydrated in dH_2O for 5 min and dehydrated by serial ethanols, 35, 50, 70, 95, 95 and 100% followed by critical dehydration using the SAMDRI-795 system (69). After dehydration, specimens were coated with Chromium using a Gatan Ion Beam Coater for 10 min and imaged by Field Emission Scanning Electron Microscope (JEOL 7401F).

Enzyme-linked immunosorbent assay

Conditioned media from cells cultured on transwells or on BrM–choroid–sclera explants were collected after 2 weeks and concentrated to equal volumes through 3 kDa Amicon filters (Millipore, Billerica, MA, USA). The fraction over 3 kDa was used to quantify C3a, CFH and CFB using ELISA kits from R&D Systems (Minneapolis, MN, USA) and Abcam, following the manufacturer's instructions. All samples were assayed at least per duplicate.

Zymography

A 10 μl of the above concentrated media was loaded onto Novex 10% gelatin gels (Life Technologies). Zymography assays were then performed per the manufacturer's instructions. Gels were scanned using the Odyssey system (Li-Cor, Lincoln, NE, USA). Gelatinase activity was quantified through the intensity of the bands with the software ImageStudioLite (Li-Cor).

Statistics

Results are expressed as mean ±SD, with $P < 0.05$ considered statistically significant. Differences between groups were compared using the Student *t*-test or ANOVA as appropriate using the GraphPad Prism software.

Authors' Contributions

R.F.G. designed and performed the experiments and wrote the manuscript. K.M.B. gave guidance on CRISPR/Cas9 experiments. E.A.P. supervised the work and reviewed and edited the manuscript.

Supplementary Material

Supplementary Material is available at *HMG* online.

Acknowledgements

The authors would like to thank Ann Tisdale for helpful technical assistance with SEM. This work was supported by the Ocular Genomics Institute.

Conflict of Interest statement. None declared.

Funding

This work was supported by the Ocular Genomics Institute.

References

1. Miller, J.W. (2013) Age-related macular degeneration revisited–piecing the puzzle: the LXIX Edward Jackson memorial lecture. *Am. J. Ophthalmol.*, **155**, 1–35.e13.
2. Evans, J.R. and Lawrenson, J.G. (2012) Antioxidant vitamin and mineral supplements for slowing the progression of age-related macular degeneration. *Cochrane Database Syst. Rev.*, **11**, CD000254.
3. Newsome, D.A., Huh, W. and Green, W.R. (1987) Bruch's membrane age-related changes vary by region. *Curr. Eye Res.*, **6**, 1211–1221.
4. Nita, M., Strzalka-Mrozik, B., Grzybowski, A., Mazurek, U. and Romaniuk, W. (2014) Age-related macular degeneration and changes in the extracellular matrix. *Med. Sci. Monit.*, **20**, 1003–1016.
5. Curcio, C.A. and Johnson, M. (2013) Structure, function, and pathology of Bruch's membrane. *Retina*, **1**, 465–481.
6. Fernandez-Godino, R., Pierce, E.A. and Garland, D.L. (2016) Extracellular matrix alterations and deposit formation in AMD. *Adv. Exp. Med. Biol.*, **854**, 53–58.
7. Macgregor, A.M., Eberhart, C.G., Fraig, M., Lu, J. and Halushka, M.K. (2009) Tissue inhibitor of matrix metalloproteinase-3 levels in the extracellular matrix of lung, kidney, and eye increase with age. *J. Histochem. Cytochem.*, **57**, 207–213.
8. Deryugina, E.I., Bourdon, M.A., Reisfeld, R.A. and Strongin, A. (1998) Remodeling of collagen matrix by human tumor cells requires activation and cell surface association of matrix metalloproteinase-2. *Cancer Res.*, **58**, 3743–3750.
9. Marin-Castan~o, M.E., Csaky, K.G. and Cousins, S.W. (2005) Nonlethal oxidant injury to human retinal pigment epithelium cells causes cell membrane blebbing but decreased MMP-2 activity. *Invest. Ophthalmol. Vis. Sci.*, **46**, 3331–3340.
10. Sorokin, L. (2010) The impact of the extracellular matrix on inflammation. *Nat. Rev. Immunol.*, **10**, 712–723.
11. Murphy, G., Nguyen, Q., Cockett, M.I., Atkinson, S.J., Allan, J.A., Knight, C.G., Willenbrock, F. and Docherty, A.J. (1994) Assessment of the role of the fibronectin-like domain of gelatinase A by analysis of a deletion mutant. *J. Biol. Chem.*, **269**, 6632–6636.

12. Shipley, J.M., Doyle, G.A., Fliszar, C.J., Ye, Q.Z., Johnson, L.L., Shapiro, S.D., Welgus, H.G. and Senior, R.M. (1996) The structural basis for the elastolytic activity of the 92-kDa and 72-kDa gelatinases. Role of the fibronectin type II-like repeats. *J. Biol. Chem.*, **271**, 4335–4341.
13. Anderson, D.H., Mullins, R.F., Hageman, G.S. and Johnson, L.V. (2002) A role for local inflammation in the formation of drusen in the aging eye. *Am. J. Ophthal.*, **134**, 411–431.
14. Hageman, G.S., Luthert, P.J., Victor Chong, N.H., Johnson, L.V., Anderson, D.H. and Mullins, R.F. (2001) An integrated hypothesis that considers drusen as biomarkers of immune-mediated processes at the RPE-Bruch's membrane interface in aging and age-related macular degeneration. *Prog. Retin. Eye Res.*, **20**, 705–732.
15. Seddon, J.M., Yu, Y., Miller, E.C., Reynolds, R., Tan, P.L., Gowrisankar, S., Goldstein, J.I., Triebwasser, M., Anderson, H.E., Zerbib, J. *et al.* (2013) Rare variants in CFI, C3 and C9 are associated with high risk of advanced age-related macular degeneration. *Nat. Genet.*, **45**, 1366–1370.
16. Hageman, G.S., Anderson, D.H., Johnson, L.V., Hancox, L.S., Taiber, A.J., Hardisty, L.I., Hageman, J.L., Stockman, H.A., Borchardt, J.D., Gehrs, K.M. *et al.* (2005) A common haplotype in the complement regulatory gene factor H (HF1/CFH) predisposes individuals to age-related macular degeneration. *Proc. Natl. Acad. Sci. U.S.A.*, **102**, 7227–7232.
17. Mullins, R.F., Russell, S.R., Anderson, D.H. and Hageman, G.S. (2000) Drusen associated with aging and age-related macular degeneration contain proteins common to extracellular deposits associated with atherosclerosis, elastosis, amyloidosis, and dense deposit disease. *FASEB J.*, **14**, 835–846.
18. Crabb, J.W., Miyagi, M., Gu, X., Shadrach, K., West, K.A., Sakaguchi, H., Kamei, M., Hasan, A., Yan, L., Rayborn, M.E. *et al.* (2002) Drusen proteome analysis: an approach to the etiology of age-related macular degeneration. *Proc. Natl. Acad. Sci.*, **99**, 14682–14687.
19. Wang, L., Clark, M.E., Crossman, D.K., Kojima, K., Messinger, J.D., Mobley, J.A. and Curcio, C.A. (2010) Abundant lipid and protein components of drusen. *PLoS One*, **5**, e10329.
20. Yehoshua, Z., de Amorim Garcia Filho, C.A., Nunes, R.P., Gregori, G., Penha, F.M., Moshfeghi, A.A., Zhang, K., Sadda, S., Feuer, W. and Rosenfeld, P.J. (2014) Systemic complement inhibition with eculizumab for geographic atrophy in age-related macular degeneration: the COMPLETE study. *Ophthalmology*, **121**, 693–701.
21. Garcia Filho, C.A., Yehoshua, Z., Gregori, G., Nunes, R.P., Penha, F.M., Moshfeghi, A.A., Zhang, K., Feuer, W. and Rosenfeld, P.J. (2014) Change in drusen volume as a novel clinical trial endpoint for the study of complement inhibition in age-related macular degeneration. *Ophthalmic Surg. Lasers Imaging Retina*, **45**, 18–31.
22. Ricklin, D. and Lambris, J.D. (2013) Complement in immune and inflammatory disorders: pathophysiological mechanisms. *J. Immunol.*, **190**, 3831–3838.
23. Mastellos, D.C., Yancopoulou, D., Kokkinos, P., Huber-Lang, M., Hajishengallis, G., Biglarnia, A.R., Lupu, F., Nilsson, B., Risitano, A.M., Ricklin, D. *et al.* (2015) Compstatin: a C3-targeted complement inhibitor reaching its prime for bedside intervention. *Eur. J. Clin. Invest.*, **45**, 423–440.
24. Qu, H., Ricklin, D., Bai, H., Chen, H., Reis, E.S., Maciejewski, M., Tzekou, A., DeAngelis, R.A., Resuello, R.R., Lupu, F. *et al.* (2013) New analogs of the clinical complement inhibitor compstatin with subnanomolar affinity and enhanced pharmacokinetic properties. *Immunobiology*, **218**, 496–505.
25. Ricklin, D., Hajishengallis, G., Yang, K. and Lambris, J.D. (2010) Complement: a key system for immune surveillance and homeostasis. *Nat. Immunol.*, **11**, 785–797.
26. Anderson, D.H., Radeke, M.J., Gallo, N.B., Chapin, E.A., Johnson, P.T., Curletti, C.R., Hancox, L.S., Hu, J., Ebright, J.N., Malek, G. *et al.* (2010) The pivotal role of the complement system in aging and age-related macular degeneration: hypothesis re-visited. *Prog. Retin. Eye Res.*, **29**, 95–112.
27. Warwick, A., Khandhadia, S., Ennis, S. and Lotery, A. (2014) Age-related macular degeneration: a disease of systemic or local complement dysregulation? *J. Clin. Med.*, **3**, 1234–1257.
28. Fu, L., Garland, D., Yang, Z., Shukla, D., Rajendran, A., Pearson, E., Stone, E.M., Zhang, K. and Pierce, E.A. (2007) The R345W mutation in EFEMP1 is pathogenic and causes AMD-like deposits in mice. *Hum. Mol. Genet.*, **16**, 2411–2422.
29. Garland, D.L., Fernandez-Godino, R., Kaur, I., Speicher, K.D., Harnly, J.M., Lambris, J.D., Speicher, D.W. and Pierce, E.A. (2014) Mouse genetics and proteomic analyses demonstrate a critical role for complement in a model of DHRD/ML, an inherited macular degeneration. *Hum. Mol. Genet.*, **23**, 52–68.
30. Fernandez-Godino, R., Garland, D.L. and Pierce, E.A. (2015) A local complement response by RPE causes early-stage macular degeneration. *Hum. Mol. Genet.*, **24**, 5555–5569.
31. Woodell, A., Jones, B.W., Williamson, T., Schnabolk, G., Tomlinson, S., Atkinson, C. and Rohrer, B. (2016) A targeted inhibitor of the alternative complement pathway accelerates recovery from smoke-induced ocular injury. *Invest. Ophthalmol. Vis. Sci.*, **57**, 1728–1737.
32. Pangburn, M.K., Schreiber, R.D. and Muller-Eberhard, H.J. (1981) Formation of the initial C3 convertase of the alternative complement pathway. Acquisition of C3b-like activities by spontaneous hydrolysis of the putative thioester in native C3. *J. Exp. Med.*, **154**, 856–867.
33. Nilsson, B. and Nilsson Ekdahl, K. (2012) The tick-over theory revisited: is C3 a contact-activated protein? *Immunobiology*, **217**, 1106–1110.
34. Hindmarsh, E.J. and Marks, R.M. (1998) Complement activation occurs on subendothelial extracellular matrix *in vitro* and is initiated by retraction or removal of overlying endothelial cells. *J. Immunol.*, **160**, 6128–6136.
35. Harboe, M. and Mollnes, T.E. (2008) The alternative complement pathway revisited. *J. Cell. Mol. Med.*, **12**, 1074–1084.
36. Leivo, I. and Engvall, E. (1986) C3d fragment of complement interacts with laminin and binds to basement membranes of glomerulus and trophoblast. *J. Cell. Biol.*, **103**, 1091–1100.
37. Andersson, J., Ekdahl, K.N., Lambris, J.D. and Nilsson, B. (2005) Binding of C3 fragments on top of adsorbed plasma proteins during complement activation on a model biomaterial surface. *Biomaterials*, **26**, 1477–1485.
38. Bexborn, F., Andersson, P.O., Chen, H., Nilsson, B. and Ekdahl, K.N. (2008) The tick-over theory revisited: formation and regulation of the soluble alternative complement C3 convertase (C3(H2O)Bb). *Mol. Immunol.*, **45**, 2370–2379.
39. Stone, E.M., Lotery, A.J., Munier, F.L., Heon, E., Piguet, B., Guymer, R.H., Vandenburgh, K., Cousin, P., Nishimura, D., Swiderski, R.E. *et al.* (1999) A single EFEMP1 mutation associated with both Malattia Leventinese and Doyne honeycomb retinal dystrophy. *Nat. Genet.*, **22**, 199–202.
40. Marmorstein, L. (2004) Association of EFEMP1 with malattia leventinese and age-related macular degeneration: a mini-review. *Ophthalmic Genet.*, **25**, 219–226.
41. Marmorstein, L.Y., Munier, F.L., Arsenijevic, Y., Schorderet, D.F., McLaughlin, P.J., Chung, D., Traboulsi, E. and Marmorstein, A.D. (2002) Aberrant accumulation of EFEMP1

underlies drusen formation in Malattia Leventinese and age-related macular degeneration. *Proc. Natl. Acad. Sci.*, **99**, 13067–13072.
42. Wyatt, M.K., Tsai, J.Y., Mishra, S., Campos, M., Jaworski, C., Fariss, R.N., Bernstein, S.L. and Wistow, G. (2013) Interaction of complement factor h and fibulin3 in age-related macular degeneration. *PLoS ONE*, **8**, e68088.
43. Klenotic, P.A., Munier, F.L., Marmorstein, L.Y. and Anand-Apte, B. (2004) Tissue inhibitor of metalloproteinases-3 (TIMP-3) is a binding partner of epithelial growth factor-containing fibulin-like extracellular matrix protein 1 (EFEMP1). Implications for macular degenerations. *J. Biol. Chem.*, **279**, 30469–30473.
44. Mali, P., Yang, L., Esvelt, K.M., Aach, J., Guell, M., DiCarlo, J.E., Norville, J.E. and Church, G.M. (2013) RNA-guided human genome engineering via Cas9. *Science*, **339**, 823–826.
45. Ran, F.A., Hsu, P.D., Wright, J., Agarwala, V., Scott, D.A. and Zhang, F. (2013) Genome engineering using the CRISPR-Cas9 system. *Nat. Protoc.*, **8**, 2281–2308.
46. Maminishkis, A., Chen, S., Jalickee, S., Banzon, T., Shi, G., Wang, F.E., Ehalt, T., Hammer, J.A. and Miller, S.S. (2006) Confluent monolayers of cultured human fetal retinal pigment epithelium exhibit morphology and physiology of native tissue. *Invest. Ophthalmol. Vis. Sci.*, **47**, 3612–3624.
47. Reale, E., Groos, S., Eckardt, U., Eckardt, C. and Luciano, L. (2009) New components of 'basal laminar deposits' in age-related macular degeneration. *Cells Tissues Organs*, **190**, 170–181.
48. Mastellos, D., Prechl, J., Laszlo, G., Papp, K., Olah, E., Argyropoulos, E., Franchini, S., Tudoran, R., Markiewski, M., Lambris, J.D. *et al.* (2004) Novel monoclonal antibodies against mouse C3 interfering with complement activation: description of fine specificity and applications to various immunoassays. *Mol. Immunol.*, **40**, 1213–1221.
49. Hewitt, A.T., Nakazawa, K. and Newsome, D.A. (1989) Analysis of newly synthesized Bruch's membrane proteoglycans. *Invest. Ophthalmol. Vis. Sci.*, **30**, 478–486.
50. Tezel, T.H., Del Priore, L.V. and Kaplan, H.J. (2004) Reengineering of aged Bruch's membrane to enhance retinal pigment epithelium repopulation. *Invest. Ophthalmol. Vis. Sci.*, **45**, 3337–3348.
51. Hulleman, J.D., Kaushal, S., Balch, W.E. and Kelly, J.W. (2011) Compromised mutant EFEMP1 secretion associated with macular dystrophy remedied by proteostasis network alteration. *Mol. Biol. Cell*, **22**, 4765–4775.
52. van der Schaft, T.L., Mooy, C.M., de Bruijn, W.C., Bosman, F.T. and de Jong, P.T. (1994) Immunohistochemical light and electron microscopy of basal laminar deposit. *Graefes Arch. Clin. Exp. Ophthalmol.*, **232**, 40–46.
53. Sarks, S., Cherepanoff, S., Killingsworth, M. and Sarks, J. (2007) Relationship of Basal laminar deposit and membranous debris to the clinical presentation of early age-related macular degeneration. *Invest. Ophthalmol. Vis. Sci.*, **48**, 968–977.
54. Chu, V.T., Weber, T., Wefers, B., Wurst, W., Sander, S., Rajewsky, K. and Kuhn, R. (2015) Increasing the efficiency of homology-directed repair for CRISPR-Cas9-induced precise gene editing in mammalian cells. *Nat. Biotechnol.*, **33**, 543–548.
55. Morrison, C.J., Butler, G.S., Rodriguez, D. and Overall, C.M. (2009) Matrix metalloproteinase proteomics: substrates, targets, and therapy. *Curr. Opin. Cell. Biol.*, **21**, 645–653.
56. Guo, L., Hussain, A.A., Limb, G.A. and Marshall, J. (1999) Age-dependent variation in metalloproteinase activity of isolated human Bruch's membrane and choroid. *Invest. Ophthalmol. Vis. Sci.*, **40**, 2676–2682.
57. Pangburn, M.K. (1983) Activation of complement via the alternative pathway. *Fed. Proc.*, **42**, 139–143.
58. Cox, T.R. and Erler, J.T. (2011) Remodeling and homeostasis of the extracellular matrix: implications for fibrotic diseases and cancer. *Dis. Model. Mech.*, **4**, 165–178.
59. Bonnans, C., Chou, J. and Werb, Z. (2014) Remodelling the extracellular matrix in development and disease. *Nat. Rev. Mol. Cell. Biol.*, **15**, 786–801.
60. Burrage, P.S., Mix, K.S. and Brinckerhoff, C.E. (2006) Matrix metalloproteinases: role in arthritis. *Front. Biosci.*, **11**, 529–543.
61. Johnson, L.V., Leitner, W.P., Rivest, A.J., Staples, M.K., Radeke, M.J. and Anderson, D.H. (2002) The Alzheimer's A beta -peptide is deposited at sites of complement activation in pathologic deposits associated with aging and age-related macular degeneration. *Proc. Natl. Acad. Sci.*, **99**, 11830–11835.
62. Tan, R.J. and Liu, Y. (2012) Matrix metalloproteinases in kidney homeostasis and diseases. *Am. J. Physiol. Renal Physiol.*, **302**, F1351–F1361.
63. Mullins, R.F., Schoo, D.P., Sohn, E.H., Flamme-Wiese, M.J., Workamelahu, G., Johnston, R.M., Wang, K., Tucker, B.A. and Stone, E.M. (2014) The membrane attack complex in aging human choriocapillaris: relationship to macular degeneration and choroidal thinning. *Am. J. Pathol.*, **184**, 3142–3153.
64. Tziakas, D.N., Chalikias, G.K., Hatzinikolaou, H.I., Stakos, D.A., Papanas, N., Tentes, I.K., Kortsaris, A.X., Maltezos, E., Hatseras, D.I. and Kaski, J.C. (2005) Levosimendan use reduces matrix metalloproteinase-2 in patients with decompensated heart failure. *Cardiovasc. Drugs Ther.*, **19**, 399–402.
65. Sivakumar, P. and Das, A.M. (2008) Fibrosis, chronic inflammation and new pathways for drug discovery. *Inflamm. Res.*, **57**, 410–418.
66. Overall, C.M. and Kleifeld, O. (2006) Tumour microenvironment - opinion: validating matrix metalloproteinases as drug targets and anti-targets for cancer therapy. *Nat. Rev. Cancer*, **6**, 227–239.
67. Maruyama, T., Dougan, S.K., Truttmann, M.C., Bilate, A.M., Ingram, J.R. and Ploegh, H.L. (2015) Increasing the efficiency of precise genome editing with CRISPR-Cas9 by inhibition of nonhomologous end joining. *Nat. Biotechnol.*, **33**, 538–542.
68. Maminishkis, A. and Miller, S.S. (2010) Experimental models for study of retinal pigment epithelial physiology and pathophysiology. *J. Vis. Exp.*, **45**, 2032.
69. Fernandez-Godino, R., Garland, D.L. and Pierce, E.A. (2016) Isolation, culture and characterization of primary mouse RPE cells. *Nat. Protoc.*, **11**, 1206–1218.
70. Sonoda, S., Spee, C., Barron, E., Ryan, S.J., Kannan, R. and Hinton, D.R. (2009) A protocol for the culture and differentiation of highly polarized human retinal pigment epithelial cells. *Nat. Protoc.*, **4**, 662–673.
71. Ho, T.C. and Del Priore, L.V. (1997) Reattachment of cultured human retinal pigment epithelium to extracellular matrix and human Bruch's membrane. *Invest. Ophthalmol. Vis. Sci.*, **38**, 1110–1118.
72. Schneider, C.A., Rasband, W.S. and Eliceiri, K.W. (2012) NIH Image to ImageJ: 25 years of image analysis. *Nat. Methods*, **9**, 671–675.